Nuclear Localization Signal Peptides Induce Molecular Delivery along Microtubules

Hanna Salman,* Asmahan Abu-Arish,* Shachar Oliel,† Avraham Loyter,† Joseph Klafter,‡ Rony Granek,§ and Michael Elbaum*

*Department of Materials and Interfaces, Weizmann Institute of Science, Rehovot 76100, Israel; †Alexander Silberman Institute of Life Sciences, The Hebrew University of Jerusalem, Givat Ram, Jerusalem 91904, Israel; ‡School of Chemistry, Tel Aviv University, Tel Aviv 69978, Israel; and §Department of Biotechnology Engineering and The Institute for Applied Biosciences, Ben Gurion University of the Negev, Beer-Sheva 84105, Israel

ABSTRACT Many essential processes in eukaryotic cells depend on regulated molecular exchange between its two major compartments, the cytoplasm and the nucleus. In general, nuclear import of macromolecular complexes is dependent on specific peptide signals and their recognition by receptors that mediate translocation through the nuclear pores. Here we address the question of how protein products bearing such nuclear localization signals arrive at the nuclear membrane before import, i.e., by simple diffusion or perhaps with assistance of cytoskeletal elements or cytoskeleton-associated motor proteins. Using direct single-particle tracking and detailed statistical analysis, we show that the presence of nuclear localization signals invokes active transport along microtubules in a cell-free *Xenopus* egg extract. Chemical and antibody inhibition of minus-end directed cytoplasmic dynein blocks this active movement. In the intact cell, where microtubules project radially from the centrosome, such an interaction would effectively deliver nuclear-targeted cargo to the nuclear envelope in preparation for import.

INTRODUCTION

Molecular exchange across the nuclear envelope takes place through the nuclear pore complexes (NPCs). Most proteins and RNAs depend on a selective transport mechanism mediated by short peptide sequences: nuclear localization signals (NLS) for import into the nucleus, and nuclear export signals (NES) for export (1). Soluble receptors of the karyopherin/importin superfamily bind these molecules and usher them across the NPC, with the GTPase Ran providing directionality (2,3).

Localization and transport in the cytoplasm occur largely via active mechanisms involving the cytoskeleton and associated motor proteins (4). Microtubules are classically associated with vesicle and organelle transport, including the endocytotic and exocytotic pathways, endoplasmic reticulum, mitochondria, and nuclear migration. In nonmuscle cells, actin-dependent transport is typically connected with processes at the plasma membrane and with force generation by polymerization, as well as with whole-cell contractility and migration. Cytoskeleton-associated vesicle movements can be observed directly in the light microscope. There is also evidence for cytoskeletal transport of nonmembranated, molecular cargo. For example, both actin and microtubules, with their associated motors, have been implicated in mRNA localization after export from the nucleus (5,6). Moving in the opposite direction, many animal viruses are known to take advantage of microtubule-based transport for delivery to the nuclear envelope, where the genome is released through the nuclear pores (7–16). Viral interaction with the cytoskeleton was reviewed recently by Campbell and Hope (17), and by Dohner and Sodeik (18). We propose here that nuclear targeting of cellular proteins in general may begin with cytoskeleton-based delivery through the cytoplasm. The microtubule network is ideally configured to support such a process, with long microtubules radiating throughout the cell from a locus near the nucleus. The slower-growing ''minus'' ends of the microtubules point toward this microtubule organizing center, whereas the ''plus'' ends face the cell periphery. In this work we test the hypothesis that the presence of an NLS is sufficient to invoke a cytoskeleton-based delivery mechanism, and in particular movement along microtubules mediated by a minus-end directed protein motor.

There exist several prior indications of microtubule involvement in delivery of nonviral nuclear import substrates or complexes. The nuclear import receptor importin α was found to associate with cytoskeleton in plant cells (19). In *Aplysia* neurons it has been shown that microtubules are required for retrograde transport of NLS-labeled proteins along the axon (20), whereas a more recent study in mammalian neurons addresses the role of microtubules in retrograde shuttling of nuclear import complexes within the axon after injury (21). The rate of nuclear accumulation of the parathyroid hormone-related protein (a nuclear transport substrate with an unconventional, direct interaction with importin-β) was reduced in cells where microtubules had been depolymerized by nocodazole (22). A similar kinetic dependence on microtubules was noted for microinjected gene delivery vectors, modified to include a site for NFκB

Submitted January 27, 2005, and accepted for publication June 15, 2005.

Address reprint requests to Michael Elbaum, Tel.: 972-8-9343537; Fax: 972-8-9344138; E-mail: michael.elbaum@weizmann.ac.il.

0006-3495/05/09/2134/12 $2.00

doi: 10.1529/biophysj.105.060160

binding so as to promote nuclear import (23). The tumor suppressor protein p53 was also found to depend on microtubules for its nuclear import (24), though not via its NLS region (25). By contrast, microtubules may act in cytoplasmic sequestration, particularly for factors involved in transcription (26–28). Important links have also been noted between key factors involved in nuclear transport and spindle microtubule assembly during mitosis (29–33). A recent study implicates molecular motors in delivery of importin-β to mitotic spindle poles (34).

To address the question presented above, we have developed a motility assay based on fluorescent particle tracking that would allow us to detect a functional interaction between an NLS-bearing cargo and cytoskeleton-associated transport. Observations are made in an interphase extract of *Xenopus laevis* eggs. The use of *Xenopus* egg extracts is well established in studies of nuclear assembly and transport on one hand, and of cytoskeletal dynamics on the other. The high-speed clarified, interphase extract used here permits us to test motility dependent on the cytoskeleton and nuclear import in parallel, in the same biochemical environment. The cytosolic fraction contains the requisite tubulin, actin, and soluble motor proteins to support cytoskeletal assembly (35,36) and a variety of active movement phenomena involving membranes (37,38), embedded particles (39), nuclear migration (40), and actin ''comet tail'' propulsion by *Listeria monocytogenes* (41). For this assay, the randomly oriented networks of F-actin and microtubules that form spontaneously in the extract serve as a lattice along which to track movements of fluorescent substrates over time. Statistical analyses are then applied to the tracking records directly, with no need for manual selection of movement events. The profitable use of entire traces enables collection of good statistics, and includes implicitly the probability of association between the tracer particle and the filament. If NLS cargo is indeed carried along microtubules or actin filaments we would expect to observe enhanced motility with respect to substrates lacking an NLS. Furthermore, this enhancement should be sensitive to depolymerization of the specific cytoskeletal components.

As potential motility substrates we employed complexes of fluorescently labeled single-stranded DNA (ssDNA) and the VirE2 protein of *Agrobacterium tumefaciens* (42,43). These complexes exist as solenoidal (''telephone cord'') structures, where the ssDNA lies along the inner diameter of a hollow, cylindrical protein shell (44,45). The ssDNA is thus protected from cytoplasmic nucleases, whereas the outer protein surface is available for biochemical interaction. An example of such a complex formed in vitro appears in Fig. 1 *A*. Single-stranded ''transfer DNA'', VirE2, and a second protein VirD2 (in single copy at the 5′ end; not used here) are involved in genetic transformation of plants (46,47). VirE2 itself contains two putative NLS regions. It is doubly suited for this study. First, by using long DNA the protein-DNA complex can be made sufficiently large to permit reliable tracking by fluorescence microscopy. Second, the putative NLSs in the wild-type protein involved in plant infection (referred to in the text as plVirE2) are not recognized in animal cells, presenting a negative control. Reversing the order of two adjacent amino acids in either NLS region results in a peptide similar to the bipartite NLS of nucleoplasmin, however. The resulting mutated, or ''animalized'' VirE2 (anVirE2) binds ssDNA and was shown to mediate nuclear import of ssDNA into *Xenopus* oocyte and *Drosophila* embryo nuclei (48). Nuclear accumulation of these complexes was blocked by protein import inhibitors (46,48,49), indicating that they employ the classic importin/Ran-mediated pathway.

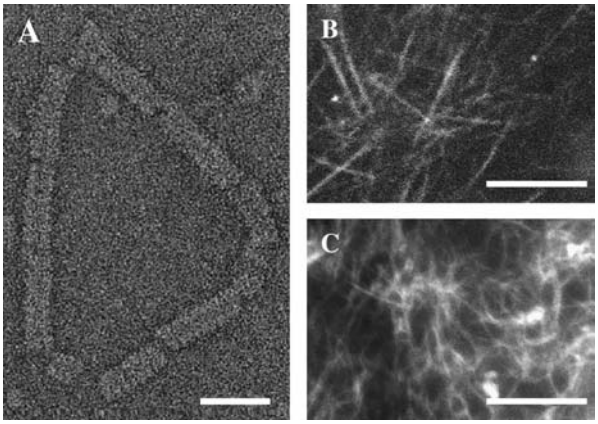

FIGURE 1 Formation of complexes and cytoskeletal networks. (*A*) Transmission electron micrograph in negative stain of a single VirE2-ssDNA complex on circular (M13) ssDNA. Structures formed by plVirE2 and anVirE2 are indistinguishable. (*B*) Fluorescent microtubule network in the high-speed centrifuged interphase *Xenopus* egg extract, imaged by confocal microscopy to emphasize the in-plane orientation. (*C*) Actin filaments also form a network in the egg extract, observed by epi-fluorescence. Scale bars 25 nm in panel *A*; 10 μm in panels *B* and *C*.

The two ssDNA-VirE2 complexes represent ideal substrates with which to test the hypothesis of cytoskeletal delivery by a particle-tracking approach. Diffusion is slow enough to permit reliable tracking, due to their size, while biochemically they differ only by the swap of two adjacent amino acids in the anVirE2. If the consequence of this swap is to activate the mechanisms of nuclear import, then we can compare the behavior of the two otherwise identical complexes to detect an activation of cytoskeletal interactions.

MATERIALS AND METHODS

Preparation of *Xenopus laevis* extracts

Following the protocol of Newmeyer and Wilson (50), female frogs were injected with 200 units pregnant mare gonadotropin, and 4–7 days later with 600–700 units human chorionic gonadotropin to induce laying the following day. (All reagents were from Sigma Israel Chemical, Rehovot, Israel.) Eggs were collected in Marc's modified ringer's buffer (NaCl 100 mM, KCl 2 mM, $CaCl_2$ 2 mM, $MgCl_2$ 1 mM, and 5 mM Hepes-NaOH, pH 7.4), dejellied gently with 2% cysteine solution (pH 8), transferred into S-lysis buffer (sucrose 250 mM, KCl 50 mM, $MgCl_2$ 2.5 mM, DTT 1 mM,

cycloheximide 50 μg/ml, and cytochalasin D 0.5 μg/ml), and packed into 2 ml centrifuge tubes. A crude extract was first prepared by centrifugation in a swinging rotor at 10,000 $\times$ g for 15 min at 4°C. A floating lipid layer and the tightly packed lowest layer were discarded, whereas the central layers containing soluble and vesicle fractions were transferred to fresh tubes and respun for 1 h at 200,000 $\times$ g and 4°C to isolate cytosolic and membrane fractions. Aliquots of this high-speed centrifuged extract were frozen in liquid nitrogen and stored at −80°C.

Preparation of cytoskeletal networks in *Xenopus* egg extract

For the dynamics measurements, the cytosolic fraction of high-speed centrifuged egg extract was mixed with an ATP regenerating system (final concentration was 1 mM ATP, 1 mM GTP, 10 mM phosphocreatine, 50 μg/ml creatine phosphokinase), and incubated at room temperature for 20 min. Microtubules and actin polymerize spontaneously under such conditions (Fig. 1, *B* and *C*; (35,36)). Small concentrations of taxol (1 μM) encourage more vigorous microtubule polymerization, without a strong effect on the network morphology. For visualization, microtubules were made fluorescent by addition of 0.1 mg/ml Oregon green tubulin (Molecular Probes, Eugene, OR) to the cytosol. Similarly, F-actin filaments were made fluorescent by addition of TRITC-actin (Cytoskeleton, Denver, CO) at 0.1 mg/ml.

Preparation of fluorescent ssDNA-VirE2 complexes

Single-stranded DNA (ϕX173 or M13mp18, New England Biolabs, Beverly, MA) was labeled covalently with Cy3 fluorophores using the LabelIt kit (Mirus, Madison, WI), per the manufacturer's instructions. After purification, it was mixed with plVirE2 (nopaline-strain; (43)) or anVirE2 ((48) s20 mutant) protein at a ratio of 20:1 w/w, protein/DNA, double the stoichiometric ratio to ensure complete coverage. The mix was incubated on ice for several hours before use.

Nuclear import assays

Cell-free nuclei were reconstituted by mixing cytosol and membrane components of the extract with demembranated *Xenopus* sperm chromatin and an ATP regeneration system (50). Competence for nuclear import of protein substrates was confirmed using fluorescent albumin labeled with a synthetic nuclear localization signal of the SV40 large T antigen (51). After assembly, fluorescent ssDNA-VirE2 complexes were added to the reaction, along with a large fluorescent dextran (167 MDa, Molecular Probes) and a second portion of the ATP regeneration system. Nuclei were observed by confocal scanning fluorescence microscopy (Olympus Fluoview 200, 60×/1.4 N.A. objective; Tokyo, Japan) after 60 min, without fixation.

Preparation of axonemes

Red Sea sea urchins (obtained from Seor-Marine, Eilat, Israel) were injected with 0.5 M KCl solution and sperm collected in a sea water solution. Axonemes were prepared following the protocol of the Vale lab (http://valelab.ucsf.edu). Briefly, sperm were pelleted by centrifugation at 2000 $\times$ g, then resuspended, demembranated, and beheaded by douncing in a buffer of 5 mM imidazole/Cl^-, pH 7.0, 100 mM NaCl, 4 mM $MgSO_4$, 1 mM $CaCl_2$, 0.1 mM EDTA, 0.1 mM ATP, 7 mM bME, containing 1% Triton X-100. Heads were sedimented first (1500 $\times$ g for 5 min), followed by three cycles of sedimentation (12,000 $\times$ g for 5 min) and resuspension. The remaining pellet was then resuspended and incubated 10 min in a high salt buffer (5 mM imidazole-Cl, pH 7.0, 600 mM NaCl, 4 mM $MgSO_4$, 1 mM $CaCl_2$, 0.1 mM EDTA, 7 mM bME, 1 mM DTT), followed by a repeated incubation in the high salt buffer with 1% Triton X-100 at pH 8.0. Finally the axoneme fragments were resuspended in the lower-salt buffer (3 cycles), brought to a suitable concentration as evaluated by differential interference contrast microscopy, aliquoted, and frozen in liquid nitrogen with 50% glycerol.

Motility on axonemes and stationary microtubules

Coverslips were prepared with adsorbed axonemes as microtubule seeds. The axonemes were deposited from thawed aliquots onto a clean coverslip and allowed to deposit. The remaining liquid was blotted and dried gently in air. A drop (4 μl) of the egg extract cytosol, to which fluorescent anVirE2-ssDNA complexes had been added, was placed on the microscope slide and closed with the coverslip. The chamber was sealed with molten wax. After incubation at room temperature, microtubules were imaged by differential interference contrast with a SensiCam QE cooled charge-coupled device camera (PCO, Kelheim, Germany) on an Olympus BX62 microscope. Image sequences were then recorded in fluorescence mode at four frames per second directly to the PC, using the camera manufacturer's software. Image analysis and processing was performed using ImageJ (available at http://rsb.info.nih.gov/ij, developed by Wayne Rasband, National Institutes of Health, Bethesda, MD).

Tracking assay

Complexes of fluorescent ssDNA with plVirE2 or anVirE2 were introduced, at room temperature, to egg cytosol in which cytoskeletal networks had been allowed to form, or alternately in which their formation was blocked by specific inhibitors (see below). The working concentration of protein-DNA complexes was 0.001 μg DNA/μl extract. A 4-μl drop of this sample mixture was sealed with molten wax between a standard glass microscope slide and an 18-mm square No. 1.5 coverslip. The thickness of the chamber so formed (~10 μm) ensures that the relatively long microtubules will be oriented approximately horizontally. The chamber was then mounted on the microscope (Olympus BX50WI, 60×/1.4 N.A. objective), at room temperature. Image sequences were recorded directly to the PC using an intensified CCD video camera (Princeton Instruments, Trenton, NJ) and a MIL-based (Matrox, Darval, Quebec, Canada) program written in-house. The optical arrangement yielded a magnification corresponding to 300 nm/pixel on the camera. The exposure time was 4/25 s, with a recording rate of 6.25 frames per second. Individual sequences were typically recorded for 40–240 s. To ensure that the data would not be corrupted by spurious effects such as leaks, air bubbles, or liquid flows in the observation chamber, recordings were taken only from samples where two or more complexes could be observed in the same field, whose motions were not correlated. Recordings were halted when the complexes moved out of focus, resulting in loss of the fluorescence signal. The image sequences were analyzed offline for centroid location, again using MIL-based routines and custom software.

Probability distribution function (PDF) histograms were calculated from the occurrences of measured excursions. For a specific interval Δt, all the distances executed by the substrate over that time difference, during the entire recording, were calculated according to the equation: $R(\Delta t) = [(x(t+\Delta t) - x(t))^2 + (y(t+\Delta t) - y(t))^2]^{1/2}$ using MATHEMATICA (Wolfram Research, Champaign, IL), where the coordinates $x(t)$ and $y(t)$ were taken from the raw output of the particle-tracking analysis. Traces from each type of complex were evaluated independently, and the measurements of $R(\Delta t)$ were binned into histograms yielding the distribution of all the displacements in that time interval Δt. The curves in Figs. 4, *A–C*, and 5, *A* and *B*, represent fits to the Gaussian PDF: $(RdR/2D(\Delta t)t)\exp[-R^2/4D(\Delta t)t]$, where $D(\Delta t)$ is the quasidiffusion coefficient of the motion, used as a fitting parameter. Mean square displacements (MSDs) were calculated from the PDFs as $\langle x^2(t)\rangle = \sum_{x=0}^{\infty} x^2 P(x,t)$.

Inhibitors of cytoskeleton and associated motor proteins

Nocodazole and cytochalasin D were added to the extract to depolymerize microtubules and F-actin, at working concentrations of 15 μM and 0.6 μg/ml,

respectively, 20 min before introduction of complexes. AMP-PNP and sodium orthovanadate were similarly added to the extract to final concentrations of 1 mM. The antidynein intermediate chain monoclonal antibody 70.1 was used at 1 mg/ml concentration. (Reagents were from Sigma Israel Chemical.) Activity of the chemical inhibitors was verified using a bead-based assay in the same extract (39).

Biochemical pulldown and immunoblotting

Cellulose beads with immobilized calf thymus single-stranded DNA (Sigma, D-8273) and DNA-free cellulose beads (Sigma, S-3504) were washed and blocked with 0.5% bovine serum albumin. Equal quantities were placed in minispin columns (Pierce, Rockford, IL). AnVirE2 and plVirE2 were introduced to the ssDNA-beads, and anVirE2 to one of the DNA-free bead columns as a control. A second control column was left with buffer only. The columns were incubated for 30 min at room temperature and then washed of free protein. *Xenopus* egg cytosol plus an ATP regenerating system were added to each column and incubated with turning overnight at 4°C. Excess cytosol was washed and bound proteins were eluted by trifluoroacetic acid and boiling. The eluates were run on SDS-PAGE gels and blotted to nitrocellulose membrane. The blots were probed with the SUK4 monoclonal antibody for kinesin (Cytoskeleton), the 74.1 monoclonal antibody for dynein intermediate chain (Chemicon, Temecula, CA), and the H-300 polyclonal antibody to importin-β (SC-11367; Santa Cruz Biotechnology, Santa Cruz, CA). Detection was made by secondary antibodies conjugated to horseradish peroxidase (Jackson Laboratories, Amritsar, India) using ECL chemi-luminescence substrate (Jackson Immunoresearch Laboratories, West Grove, PA). Recognition of the antigens in the *Xenopus* egg extract was confirmed by comparison in test blots with HeLa cell extract. The SUK4 antibody recognized two closely spaced bands alongside a single band in HeLa cell extract.

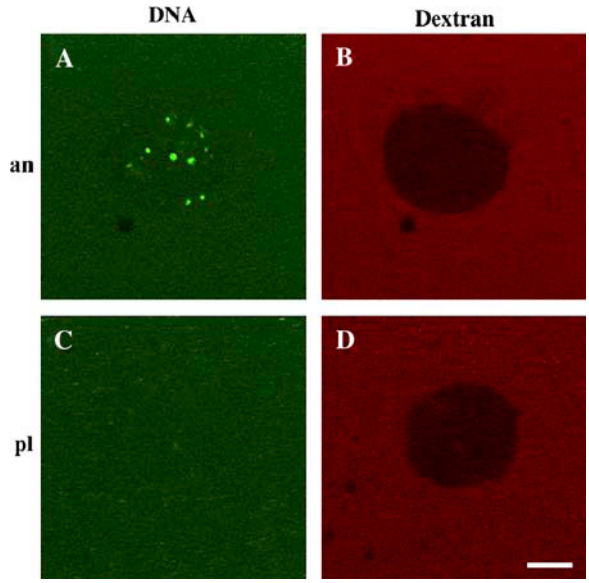

FIGURE 2 Nuclear import of ssDNA-anVirE2 complex, imaged by scanning fluorescence confocal microscopy, with fluorescent molecules as marked: VirE2 with fluorescein-labeled ssDNA and 167 kDa TRITC-dextran in the left and right columns, respectively. Each row shows the same nucleus in two color channels. Panel *A* shows that complexes formed with the ''animalized'' mutant anVirE2 are imported to the nucleus, whereas panel *C* shows that those formed with the wild-type plVirE2 protein are not. Panels *B* and *D* demonstrate integrity of the nuclear envelope for the same two nuclei in panels *A* and *C*, by exclusion of large fluorescent dextrans. Scale bar = 5 μm.

RESULTS

Import of VirE2-ssDNA to reconstituted nuclei

Complexes formed with ssDNA and either anVirE2 or plVirE2 were tested for nuclear import using cell-free nuclei reconstituted in vitro in *Xenopus* egg extract (52–56). After assembly, ssDNA-anVirE2 (or ssDNA-plVirE2) complexes were added and incubated for 1 h before observation at room temperature. As expected based on previous observations in other systems (48), we found that complexes formed with the anVirE2 protein containing the modified, active nuclear localization signal, accumulated inside the nuclei, whereas those formed with the wild-type plVirE2 protein did not (Fig. 2).

Presence of NLS invokes movement on microtubules in *Xenopus* egg extract

Complexes of anVirE2 and plVirE2 were prepared on fluorescent ssDNA and introduced into cytoskeletal networks reconstituted in *Xenopus* egg cytosol. Automated single-particle tracking methods were applied to follow the fluorescent complexes under the microscope to test for active movement along cytoskeletal filaments. (Nuclei were not present in these tracking experiments.) The first indication for driven motion in the case of the anVirE2 complex was seen in comparing the total path it executes over a given time with that executed by the plVirE2 complex. Examples appear in Fig. 3 *A*, where it is clear that the animalized complex explores a wider area than that formed by plVirE2. Also notable was the tendency of the anVirE2 complexes to remain in the focal plane longer than those formed with plVirE2. This is consistent with a tethering of the anVirE2 complexes to microtubules, which orient approximately horizontally in the thin observation chamber. The plVirE2 complexes drifted out of focus (i.e., vertically) more quickly than the anVirE2. Sample movies appear as Supplementary Material.

To verify anVirE2 movements along stationary microtubules, we first confirmed by photobleaching that microtubules do not glide on the glass surface in clarified cytosol, consistent with earlier observations under similar conditions (35). We then prepared an observation chamber with sea urchin axoneme segments anchored to the coverslip. AnVirE2-ssDNA complexes were introduced, along with egg extract, and the chamber was sealed. A still image of the axonemes and microtubules that nucleated from them was recorded first using differential interference contrast, followed immediately by image sequences in fluorescence. It was then straightforward to overlay the images and to select examples of directed motion along a filament, a distinctive example of which appears in Fig. 3 *B*. Directed traces were typically shorter than 2 μm, with instantaneous velocities between 1.0 and 1.5 μm in agreement with published data (57–59).

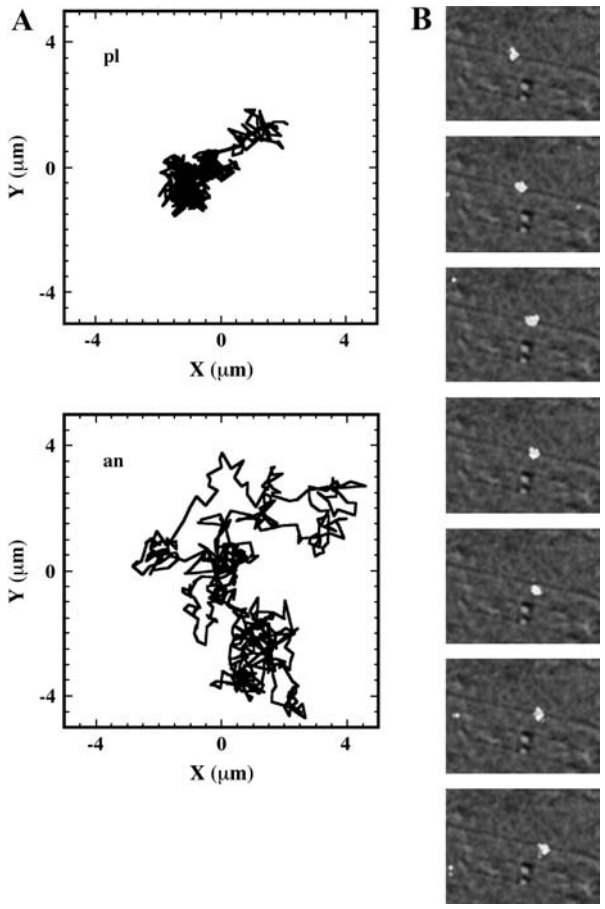

FIGURE 3 (*A*) Examples of paths executed by plant (*pl*) and animalized (*an*) (wild-type and mutant, respectively) complexes on equal times of 100 s. Note the wider area explored by the anVirE2 complex. (*B*) Microtubules and axonemes adsorbed to the glass surface are visible by differential interference contrast imaging. A fluorescent spot is observed in motion along a track. Horizontal field = 13 μm. Time interval 0.25 s per frame.

Rather than collecting data from intermittent, selected movements, we took a statistical approach based on tracking of entire paths. A random orientation of the filament networks provides a distinct advantage in that there is no particular start or finish, other than the appearance or disappearance of a particle from the focal plane. Segments of the detected traces may therefore be accumulated together because they represent equivalent information. Comparisons among these statistical distributions, prepared from traces made under differing conditions, can then be made objectively. Notably, a meaningful signal is obtained even when the effect in question is absent. This possibility of a rigorous negative control is a significant technical advantage to the method.

Each trace of a VirE2-ssDNA particle is quantified by two spatial coordinates and one temporal coordinate: x, y, and t. From this list the displacements $\vec{r}$ are evaluated for all instances of a given time interval Δt. A histogram of their lengths $R(\Delta t)$ represents a probability distribution function, whose amplitude describes the probability to move by a distance R on the relevant time Δt. A second important statistic is the mean square displacement, which describes the rate at which the particle's trajectory spreads to visit new area. The MSD is expressed in two dimensions as $\langle(\vec{r})^2\rangle = 4Dt^{\gamma}$. Ordinary diffusion (of thermal origin or otherwise) has a scaling exponent $\gamma = 1$, where D is a conventional diffusion constant with units [length]^2/[time]. Exponents $\gamma > 1$ or <1 define super- and subdiffusion, respectively; in these cases D defines a quasidiffusion coefficient that describes the rate of spreading subject to the anomalous scaling. For the purpose of comparison, the quasidiffusion coefficient measured at time interval Δt relates to the prefactor in the mean square displacement by a factor $4\Delta t^{1-\gamma}$.

Normalized probability distribution functions for the plVirE2 and anVirE2 complexes are shown in Fig. 4, *A* and *B*, evaluated at a 20-s time interval. The wider histogram and shifted peak in the case of the animalized complex indicates that it reaches longer distances than the plant complex in the same time interval. Upon depolymerizing the microtubules by nocodazole, however, the movement of the anVirE2 complex became nearly identical to that of the plant type as seen in Fig. 4 *C*. The histograms are fit to the Gaussian PDF for an uncorrelated random walk with a quasidiffusion coefficient D (for $\Delta t = 20$ s). The value of D obtained for the animalized complex in the presence of microtubules is much larger than that observed for the wild-type complex (plVirE2) in the presence of microtubules, or for the animalized complex with depolymerized microtubules. (D characterizes the shape of the distribution, and can be used for comparison in this and the following assays.) Note, too, that the tail of the anVirE2 complex distribution extends to roughly twice the distance of the plVirE2 complex, i.e., 8 vs. ~4 μm. Comparison among these distributions indicates an active transport mechanism that is dependent on both microtubules and an active nuclear localization signal.

The mean square displacement of the motions may be extracted from the same data. We see in Fig. 4 *D* that the MSD of the plVirE2, as well as the anVirE2 complexes in the microtubule-free extract, exhibit subdiffusive scaling $\langle x^2\rangle \sim t^{3/4}$ and almost identical prefactors, whereas in the presence of microtubules the animalized complex exhibits a linear scaling in time. Again, the difference in motility distinguishing complexes with anVirE2 from plVirE2 requires microtubules.

Inhibitors implicate dynein in active movement on microtubules

We next attempted to suppress activity of the distinct motor families that associate with microtubules. If active movements were dependent on kinesin, the ATP analog AMP-PNP should anchor the anVirE2 complexes to microtubules (60,61) and inhibit movement. In fact, no change in the

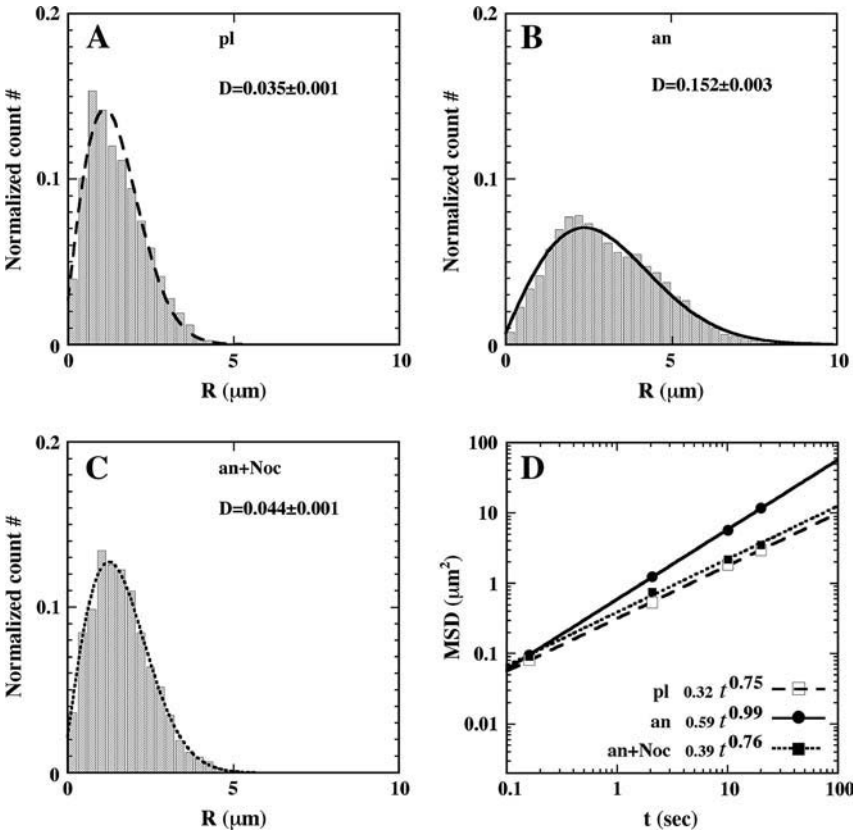

FIGURE 4 Differences between movement characteristics of the two VirE2-ssDNA complexes. Panels *A–C* are the probability distribution function histograms of the protein-DNA complex movements in the extract, for time interval of 20 s (see Materials and Methods). (*A*) plVirE2 complex in an untreated sample (6593 points from 20 traces). (*B*) anVirE2 complex in an untreated sample (18,359 points from 11 traces). (*C*) anVirE2 complex in a sample treated with nocodazole to depolymerize microtubules (3631 points from 15 traces). Curves are fits to the Gaussian PDF as described in the text, using a quasidiffusion coefficient D as the fitting parameter. (*D*) Mean square displacements (*MSD*) of the same experiments in panels *A* (□), *B* (●), and *C* (■). Lines are best fits to the data, using the same dash schemes as above. Fitting expressions are also shown, where $\langle x^2 \rangle \sim t^{\gamma}$. The quasidiffusion coefficient relates to the ordinary diffusion coefficient via a factor of $t^{1-\gamma}$.

animalized substrate movement was observed in the presence of this inhibitor: the PDF histogram was unchanged, with a quasidiffusion coefficient similar to that in the untreated extract (compare Figs. 5 *A* and 4 *B*). The MSD of anVirE2-ssDNA complexes with AMP-PNP is also similar to the untreated case (compare Figs. 5 *C* and 4 *D*). In contrast, inhibition of dynein activity by sodium orthovanadate (62) effectively restricted the movement of the anVirE2-ssDNA complex, so that it strongly resembled that of the plant type (compare Figs. 5 *B* and 4 *A*). The MSD indicates, as well, a more restricted movement resembling the MSD of the plant complex, with $t^{3/4}$ scaling (see Fig. 5 *C*) similar to that seen in Fig. 4 *D* with plVirE2 or anVirE2 with depolymerized microtubules. Blocking dynein function by means of monoclonal antidynein antibody 70.1 (59,63,64) had an effect identical to vanadate in the MSD of the anVirE2-ssDNA complex, as seen in Fig. 5 *C*. Thus, the supplementary movement observed for the VirE2-ssDNA complex in Fig. 4 *B* is dependent, in addition to microtubules and to the NLS in the anVirE2 protein, on functionality of the dynein motor.

Subdiffusion in the absence of active transport is related to F-actin

For cases where microtubule-dependent active movement is absent, the MSDs in Figs. 4 *D* and 5 *C* show a subdiffusive scaling of $t^{3/4}$. This recalls a number of earlier observations related to networks of semiflexible filaments, and actin in particular (65–68). To test whether the effect is indeed due to filamentous actin, we added cytochalasin D to the extract to disrupt the actin network, and retested the behavior of plVirE2 complexes. In that case we found ordinary diffusion scaling (Fig. 5 *D*). Conditions of simultaneous actin and microtubule depolymerization yielded nearly identical results. Lacking actin or microtubule filaments, we attribute these observations to ordinary Brownian motion in a fluid medium. The passive subdiffusion of plVirE2 in the presence of F-actin thus provides an additional signature of the active motion of anVirE2 along microtubules. Cytochalasin alone does not affect the movement of anVirE2 in the presence of microtubules.

Pulldown from extract brings dynein and importin-β but not kinesin

To confirm the presence of dynein on the moving complexes, and also to investigate whether kinesin may be present in addition, we performed a pulldown assay using ssDNA immobilized on small columns of cellulose beads. AnVirE2 and plVirE2 were introduced to the ssDNA beads to form the respective complexes, and then the beads were incubated in the *Xenopus* egg extract. Two types of DNA-free cellulose beads were used as control, with one batch left blank and the

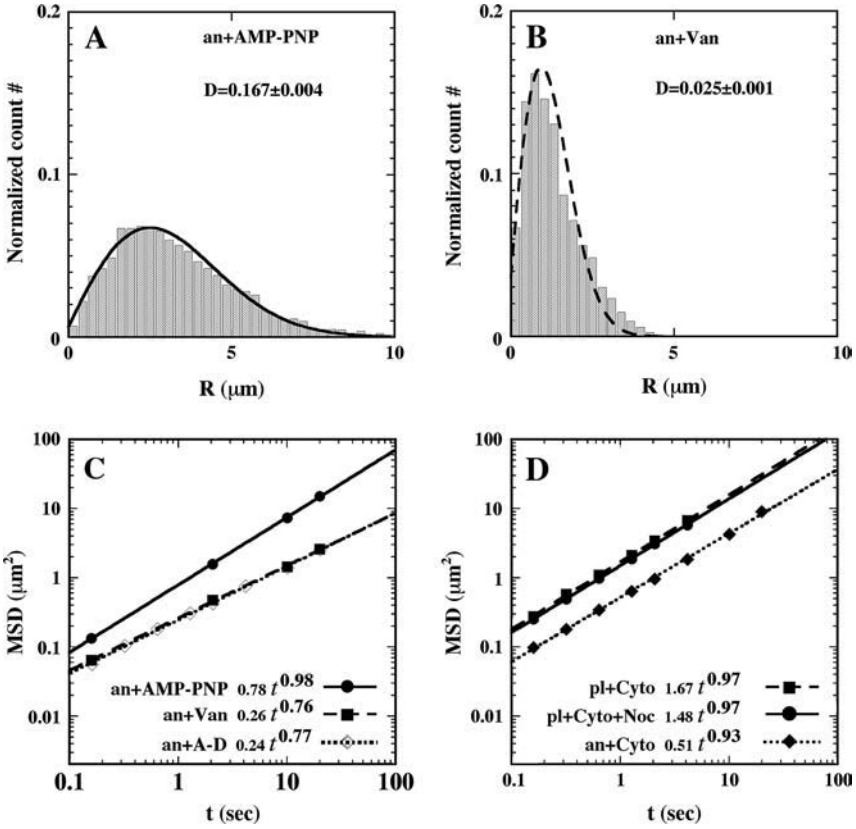

FIGURE 5 Effect of motor protein inhibition on the (mutant) anVirE2 complex behavior. (*A*) PDF histogram (11,929 points from 20 traces) of the animalized complex with kinesin activity suppressed by AMP-PNP. (*B*) PDF histogram (12,193 points from 27 traces) where dynein was inhibited by sodium orthovanadate. Curves in both cases are best fits to the Gaussian PDF with quasidiffusion coefficient D indicated in each graph. (*C*) MSD for three cases: kinesin inhibition by AMP-PNP (●, *solid line*), dynein inhibition by vanadate (■, *dashed line*), and inhibition of dynein by antidynein antibody (◇, *dotted line* overlapping *dashed*). (*D*) Restoration of classical Brownian motion for plant complex by F-actin disruption (■) and additionally microtubule depolymerization (●). Diamonds show the MSD of the mutant complex movement with depolymerized F-actin. Expressions for power-law fits are displayed in panels *C* and *D* as in Fig. 4 *D*. Note the close match of the plVirE2 results shown here, indicating the absence of interaction with microtubules, and the similarity between the anVirE2 result shown here and that in Fig. 4 *D*, in the presence of F-actin, as the microtubule-driven motion is not hindered by the actin network.

other exposed to anVirE2 (and subsequently washed) before introduction to the extract. After overnight incubation at 4°C, bound proteins were eluted by trifluoroacetic acid and boiling. The four eluates were analyzed by SDS-PAGE and Western blotting, using antibodies to dynein intermediate chain (mAb 74.1) and to conventional kinesin (SUK4). Blots were additionally tested for importin-β (SC-11367). Importin-β was recognized specifically on anVirE2 complex, though with a significant background level in the control lanes. Surprisingly, dynein appeared in both anVirE2- and plVirE2-column eluates, suggesting that at least a part of the multichain dynein motor may be present on the plVirE2-ssDNA complexes as well as the anVirE2-ssDNA complexes. We saw no evidence for kinesin even at very high exposure of the film. These results appear in Fig. 6.

DISCUSSION

The results presented here demonstrate a functional link between the presence of a nuclear localization signal and dynein-dependent transport along microtubules. We have shown by direct particle tracking and statistical analysis that a nucleoprotein complex containing nuclear localization signals (anVirE2-ssDNA) is both imported to reconstituted nuclei and driven along microtubules by dynein, where a similar complex lacking the NLS (plVirE2-ssDNA) is neither imported to nuclei nor driven along microtubules. Physiologically, the VirE2 protein employed is involved in gene transfer by *Agrobacterium tumefaciens*. Activity of the wild-type protein is limited to plants, however, due to interaction with the plant-specific host factor VIP1 (49). The ''animalized'' anVirE2 is mutated by a simple exchange in the order of two adjacent amino acids, the consequence of which is to engineer an effective NLS similar to that of

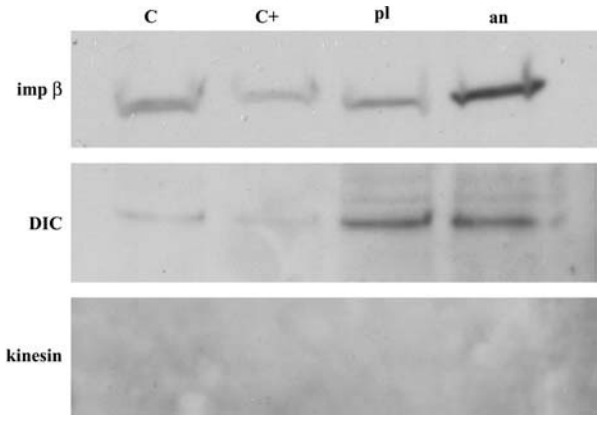

FIGURE 6 Western blots from pulldowns using VirE2-ssDNA immobilized on beads. Importin-β appears specifically on the anVirE2-ssDNA. Dynein intermediate chain (*DIC*) appears on both anVirE2- and plVirE2-ssDNA complexes. Kinesin is not detected.

nucleoplasmin. Such ''classical'' NLS sequences induce nuclear import in the *Xenopus* egg extract by recruiting the importin-α/β nuclear import receptors. This same exchange mutation in VirE2 induces, as well, the dynein-dependent movements along microtubules.

Directed movements of anVirE2-ssDNA complexes can be observed straightforwardly on anchored axonemes and microtubules. Analysis of these movements, however, inevitably involves a subjective distinction between true directed motion along the filament and a diffusive passage nearby. The disordered cytoskeletal networks that form spontaneously in the *Xenopus* egg extract suggest an alternate approach based on random walk analysis, which we pursued. It is particularly relevant to kinetics of cytoplasmic dynein motors, which are known for their limited processivity and even directional fidelity (57,58).

Active movement of anVirE2-ssDNA complexes on microtubules was revealed by comparing probability distribution functions and mean square displacement statistics with those obtained when microtubules were depolymerized by nocodazole. These statistical measures, when applied to traces of plVirE2-ssDNA complexes in the presence of microtubules, were essentially identical to those of anVirE2-ssDNA without microtubules. Thus, we conclude that plVirE2 does not associate with or move along microtubules. Disruption of filamentous actin by cytochalasin D had no effect on the anVirE2-ssDNA movement, confirming the involvement of microtubules rather than actin-associated motors. Simultaneous application of nocodazole and cytochalasin led to ordinary Brownian motion with similar parameters for both types of complexes. Notably too, the plVirE2-ssDNA complex with cytochalasin alone behaved similarly to anVirE2-ssDNA with cytochalasin and nocodazole together. (The extrapolated diffusion constant is consistent with conventional Stokes-Einstein diffusion of similarly sized particles in a medium several times more viscous than water.) This provides further evidence that the plVirE2-ssDNA complex with cytochalasin moves by Brownian diffusion even in the presence of microtubules.

Given the dependence on microtubules, the active motion could be induced by kinesin-family motors or by cytoplasmic dynein. Kinesins are subject to inhibition of the motor activity by AMP-PNP (60,61), addition of which had no measurable effect on the anVirE2 complex movement. The active movement was eliminated, on the other hand, when dynein activity was blocked by vanadate ions or by a function-inhibiting antibody. In such cases the movement of anVirE2 was nearly identical to that of the plVirE2 complexes. If different at all it was more restricted, suggesting a partial binding of the anVirE2 complexes to the microtubules. Attribution of the motion to dynein motors was corroborated by a pulldown from the extract using complexes of VirE2 assembled onto ssDNA beads. Western blotting found a dynein intermediate chain on the complexes. Intriguingly, it appeared on both anVirE2 and plVirE2 complexes. Combined with the functional assays this suggests a difference in the regulation rather than recruitment of the dynein motor, governed ultimately by the nuclear localization signal. Dynein is known to be regulated by dynactin, as well as by phosphorylation, both of which may be implicated in movement of vesicles (58,69,70). A less interesting possibility is that the configuration of immobilized ssDNA on the beads may permit a broader range of protein interactions than occur in solution. The negative observation for kinesin is in this sense the more conclusive result; there is no adsorption to the DNA beads, as there is no effect of AMP-PNP in the functional assay.

Considering the relevance of these experiments to intracellular transport, dynein-mediated movements of classical NLS-bearing protein cargos would bring them toward the nuclear envelope in preparation for import. A paradoxical result is that the time course of such effects as observed in living tissue culture cells (see Introduction) is on the scale of 1 h, where a processive movement of dynein motors at their canonical micrometer-per-second rates should move cargo across the cytoplasm in a few seconds. The discrepancy is consistent with a picture of short directed movements interspersed with periods of diffusion or entrapment (71). Microtubules also support a variety of filament and membrane obstacles to diffusion in the cytoplasm, so that motor recruitment may be needed to pass obstacles that are established in part by the microtubules themselves.

In this experiment with a membrane-clarified egg extract, the most prominent barrier to diffusion in the cytosol is most likely the filamentous actin network (72). It plays an interesting role in hindering free diffusion of the complexes. Mean square displacements of all the measurements are shown in Table 1. Ordinary scaling $\langle x^2 \rangle \sim t$ is observed for the dynein-driven movements (No. 1–3) in the random network and for Brownian motion when actin is depolymerized (No. 4,5), though with very different prefactors between the two groups. In all cases without active microtubule-based transport and without cytochalasin, i.e., for plVirE2 (No. 6), or anVirE2 with nocodazole (No. 7) or with dynein inactivated (No. 8,9), the MSDs show subdiffusion with scaling as $\langle x^2 \rangle \sim t^{3/4}$. This scaling is associated with movement in a medium dominated by thermal undulations of semiflexible polymers. The phenomenon may be attributed to the existence of long decay times in the viscoelastic response, which presents essentially a time-dependent viscosity (73). Crowding in the cytoplasm will be particularly detrimental to free diffusion of relatively large virus particles (74). The observation that nuclear targeting induced by the classical nuclear localization signals themselves suggests that viral exploitation of cytoskeletal transport may represent a tuning of existing interactions rather than development of a specialized mechanism de novo.

We might have anticipated that active motility would yield a superdiffusive MSD scaling $\langle x^2 \rangle \sim t^{\gamma}$ with $\gamma > 1$. In the following we present a statistical model for the observed

TABLE 1 Summary of mean square displacement measurements, $\langle x^2 \rangle = D\,t^{\gamma}$, for the VirE2-ssDNA complexes under various treatments of the extracts

Experiment No.	Substrate	Conditions	Prefactor	Exponent-γ	Movement
1	anVirE2	Untreated	0.59	0.99	Active
2	anVirE2	+ AMP-PNP	0.78	0.98	Active
3	anVirE2	+ Cytochalasin D	0.51	0.93	Active
4	plVirE2	+ Cytochalasin D	1.67	0.97	Passive Brownian
5	plVirE2	+ Cytochalasin D + Nocodazole	1.48	0.97	Passive Brownian
6	plVirE2	Untreated	0.32	0.75	Passive restricted
7	anVirE2	+ Nocodazole	0.39	0.76	Passive restricted
8	anVirE2	+ Vanadate	0.26	0.76	Passive restricted
9	anVirE2	+ Antidynein	0.24	0.77	Passive restricted

Note that the measured exponents-γ cluster near either unity or 3/4. Active movement of the anVirE2 complexes (No. 1–3) always shows $\gamma \approx 1$, consistent with directed movement along a random network as explained in the text. Cases of thermally driven motion (No. 4,5) yield $\gamma \approx 1$ when F-actin has been depolymerized and $\gamma \approx 3/4$ when F-actin is present (No. 6–9).

active motion. The case of intermingled diffusion and motor-driven movement along a single filament has been studied in detail (75). Here, the dynein-driven movement induces a directed walk along a random network of microtubules (Fig. 7 *A*). Subtly different from a classical random walk in that the orientation of each track and the direction of movement along it are predetermined, this situation is described by a random velocity field model (76). Changes in directionality occur primarily at junctions in the network, where the complex may randomly move to an intersecting microtubule. A simple scaling approach extends the model to the present conditions of interest. Microtubules are oriented approximately horizontally, while the network is embedded in three dimensions at the points of intersection because crossing occurs to an adjacent microtubule above or below. Let x and y axes lie in the plane of microtubule orientation, with z perpendicular to the plane. We assume for simplicity (but without loss of generality) that the tracks lie along the x and y axes and appear in alternating order along the z axis, i.e., a track along the x axis meets at an intersection with two tracks along the y axis, one lying above it and the other below. Motion along the z axis will be a true random walk between tracks characterized by a diffusion constant $D_z = l^2/2\tau$, where l is the mesh size (i.e., the distance between intersections) and τ is the hopping time. Assuming that a change of tracks occurs at every junction, $\tau = l/v$ and $D_z = (vl)/2$, where v is the mean velocity of the motors along a given track. Consider first the MSD for motion along the x axis. According to the random velocity model (76), $\langle x^2(t)\rangle \approx P_{yz}(0,t)l^2v^2t^2$, where $P_{yz}(0,t)$ is the probability of return to the origin in the y-z plane, which scales as $P_{yz}(0,t) \approx (1/\sqrt{\langle y^2(t)\rangle})(1/\sqrt{D_z t})$. Because x and y are equivalent we have $\langle x^2(t)\rangle = \langle y^2(t)\rangle$, which allows to solve for $\langle x^2(t)\rangle$ and thus for $\langle \vec{r}^2(t)\rangle$. This leads to $\langle \vec{r}^2(t)\rangle \approx (lv)t$, where the numerical prefactor has been omitted. A more accurate calculation based on the treatment of Zumofen et al. (76) yields: $\langle \vec{r}^2(t)\rangle \approx A\,(lv)\,t[\ln(t/\tau)]^{2/3}$, where $A = 2^{1/3}(3/\pi)^{2/3} \simeq 1.22$. Remarkably, we obtain a result reminiscent of a simple random walk over steps whose length is the average spacing between junctions, i.e., the network mesh size l. The MSD of the random walker is given by $\langle \vec{r}^2(t)\rangle = (l^2/\tau)t$ where $\tau = l/v$ is the hopping time, leading to $\langle \vec{r}^2(t)\rangle = (lv)t$.

We may compare this prediction with numerical estimates. For the mesh size of the microtubule network, we assume that there are three microtubule filaments in each unit volume defined by the mesh size l. Each microtubule consists of $13\times l/(8\,\mathrm{nm})$ tubulin dimers (8 nm being the length of one tubulin heterodimer and 13 the protofilament number). This yields $C = (3l\times 1625)/l^3$, where l is measured in micrometers. Assuming a concentration $C = 20\,\mu$M of tubulin, solving for l yields $l = 0.62\ \mu$m. Note the very weak dependence of l on the concentration. Thus, for $t > \tau$, the expression above effectively yields $\langle \vec{r}^2(t)\rangle \approx 0.7t$, in good agreement with the observations for anVirE2 (Fig. 4 *D*) and anVirE2 + AMP-PNP (Fig. 5 *C*).

In summary, we have demonstrated an integration of the microtubule delivery and nucleocytoplasmic transport systems in an established animal cell model. A reversal in the order of two adjacent amino acids in a putative nuclear localization signal region distinguishes the anVirE2 from the wild-type plVirE2, conferring both nuclear import activity and the microtubule interaction. We conclude that the same NLS responsible for translocation through the nuclear pores also invokes an active, dynein-mediated transport along microtubules. Active movement within a disordered microtubule network yields long traces amenable to an unbiased statistical analysis. In the absence of motor-driven movements we observe a restricted diffusion that is attributed to the surrounding gel of F-actin. This suggests a physiological role for microtubule-based transport in assisting the passage of protein complexes around intracellular obstacles or through filamentous networks in a directed manner, where thermal diffusion alone might leave them trapped for long times in small cages. In the intact cell the microtubule network radiates from the centrosome near the nucleus with the plus end pointing toward the cell periphery (see Fig. 7 *B*). In this orientation, the involvement of dynein

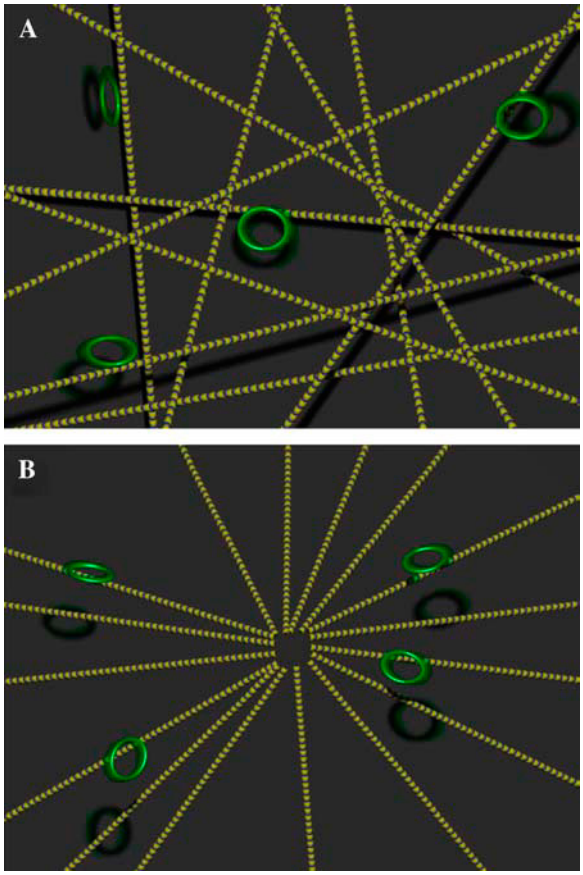

FIGURE 7 Dynein-driven movement in the random network implies retrograde movement in a radial one. (*A*) Schematic view of microtubules in the extract. Plus (*blue*) and minus (*yellow*) ends are oriented at random. VirE2-ssDNA complexes are depicted for simplicity as rings. Motor inhibition shows that they move in the plus to minus direction depicted. Because the network is random, however, no net directed movement is induced ($\langle x \rangle = 0$). Motor activity may nonetheless be deduced by statistical analysis. (*B*) Interphase microtubules normally radiate from the centrosome near the nucleus in animal cells. Motor movement becomes retrograde, carrying nuclear-targeted cargo toward the nuclear envelope.

would tend to bring the NLS-bearing substrates toward the nuclear envelope, concentrating them there for subsequent nuclear import via the conventional importin-mediated pathway.

SUPPLEMENTARY MATERIAL

An online supplement to this article can be found by visiting BJ Online at http://www.biophysj.org.

The authors are grateful to V. Citovsky for the gift of VirE2 plasmids, to D. Fass for assistance with protein expression, to Shlomit Hanz and Mike Fainzilber for help with Western blotting, to Ziv Reich, Amnon Harel, Tzvi Tzfira, and Michael Sheetz for stimulating discussions, and to Douglass Forbes for a critical reading of the manuscript.

This work was supported in part by grants from the Israel Science Foundation-The Charles H. Revson Foundation, the Minerva Research Foundation, and the Human Frontiers Science Program, and by the Gerhard M. J. Schmidt Center for Supramolecular Architecture. A.L. acknowledges support of the United States-Israel Binational Science Foundation.

REFERENCES

1. Gorlich, D., and U. Kutay. 1999. Transport between the cell nucleus and the cytoplasm. *Annu. Rev. Cell Dev. Biol.* 15:607–660.
2. Kalab, P., K. Wei, and R. Heald. 2002. Visualization of a Ran-GTP gradient in interphase and mitotic *Xenopus* egg extracts. *Science.* 295:2452–2456.
3. Smith, A. E., B. M. Slepchenko, J. C. Schaff, L. M. Loew, and I. G. Macara. 2002. Systems analysis of Ran transport. *Science.* 295:488–491.
4. Hirokawa, N. 1998. Kinesin and dynein superfamily proteins and the mechanism of organelle transport. *Science.* 279:519–526.
5. Tekotte, H., and I. Davis. 2002. Intracellular mRNA localization: motors move messages. *Trends Genet.* 18:636–642.
6. Lopez de Heredia, M., and R.-P. Jansen. 2004. mRNA localization and the cytoskeleton. *Curr. Opin. Cell Biol.* 16:80–85.
7. Sodeik, B., M. W. Ebersold, and A. Helenius. 1997. Microtubule-mediated transport of incoming herpes simplex virus 1 capsids to the nucleus. *J. Cell Biol.* 136:1007–1021.
8. Suomalainen, M., M. Y. Nakano, S. Keller, K. Boucke, R. P. Stidwill, and U. F. Greber. 1999. Microtubule-dependent plus- and minus-end directed motilities are competing processes for nuclear targeting of adenovirus. *J. Cell Biol.* 144:657–672.
9. Ye, G. J., K. T. Vaughan, R. B. Vallee, and B. Roizman. 2000. The herpes simplex virus 1 UL34 protein interacts with a cytoplasmic dynein intermediate chain and targets nuclear membrane. *J. Virol.* 74:1355–1363.
10. Seisenberger, G., M. U. Ried, T. Endress, H. Buning, M. Hallek, and C. Brauchle. 2001. Real-time single-molecule imaging of the infection pathway of an adeno-associated virus. *Science.* 294:1929–1932.
11. Suomalainen, M., M. Y. Nakano, K. Boucke, S. Keller, and U. F. Greber. 2001. Adenovirus-activated PKA and p38/MAPK pathways boost microtubule-mediated nuclear targeting of virus. *EMBO J.* 20:1310–1319.
12. Dohner, K., A. Wolfstein, U. Prank, C. Echeverri, D. Dujardin, R. Vallee, and B. Sodeik. 2002. Function of dynein and dynactin in herpes simplex virus capsid transport. *Mol. Biol. Cell.* 13:2795–2809.
13. Mabit, H., M. Y. Nakano, U. Prank, B. Saam, K. Dohner, B. Sodeik, and U. F. Greber. 2002. Intact microtubules support adenovirus and herpes simplex virus infections. *J. Virol.* 76:9962–9971.
14. McDonald, D., M. A. Vodicka, G. Lucero, T. M. Svitkina, G. G. Borisy, M. Emerman, and T. J. Hope. 2002. Visualization of the intracellular behavior of HIV in living cells. *J. Cell Biol.* 159:441–452.
15. Suikkanen, S., T. Aaltonen, M. Nevalainen, O. Välilehto, L. Lindholm, M. Vuento, and M. Vihinen-Ranta. 2003. Exploitation of microtubule cytoskeleton and dynein during parvoviral traffic toward the nucleus. *J. Virol.* 77:10270–10279.
16. Kelkar, S. A., K. K. Pfister, R. G. Crystal, and P. L. Leopold. 2004. Cytoplasmic dynein mediates adenovirus binding to microtubules. *J. Virol.* 78:10122–10132.
17. Campbell, E. M., and T. J. Hope. 2003. Role of the cytoskeleton in nuclear import. *Adv. Drug Deliv. Rev.* 55:761–771.
18. Dohner, K., and B. Sodeik. 2005. The role of the cytoskeleton during viral infection. *Curr. Top. Microbiol. Immunol.* 285:67–108.
19. Smith, H. M. S., and M. S. Raikhel. 1998. Nuclear localization signal receptor importin alpha associates with the cytoskeleton. *Plant Cell.* 10:1791–1799.
20. Ambron, R. T., R. Schmied, C. Huang, and M. Smedman. 1992. A signal sequence mediates the retrograde transport of proteins from the axon periphery to the cell body and then into the nucleus. *J. Neurosci.* 12:2813–2818.

21. Hanz, S., E. Perlson, D. Willis, J. Q. Zheng, R. Massarwa, J. J. Huerta, M. Koltzenburg, M. Kohler, J. van-Minnen, J. L. Twiss, and M. Fainzilber. 2003. Axoplasmic importins enable retrograde injury signaling in lesioned nerve. *Neuron*. 40:1095–1104.
22. Lam, M. H. C., R. J. Thomas, K. L. Loveland, S. Schilders, M. Gu, T. J. Martin, M. T. Gillespie, and D. A. Jans. 2002. Nuclear transport of parathyroid hormone (PTH)-related protein is dependent on microtubules. *Mol. Endocrinol.* 16:390–401.
23. Mesika, A., V. Kiss, V. Brumfeld, G. Ghosh, and Z. Reich. 2005. Enhanced intracellular mobility and nuclear accumulation of DNA plasmids associated with a karyophilic protein. *Hum. Gene Ther.* 16:200–208.
24. Giannakakou, P., D. L. Sackett, Y. Ward, M. Blagosklonny, and T. Fojo. 2000. P53 is associated with cellular microtubules and is transported to the nucleus by dynein. *Nat. Cell Biol.* 2:709–717.
25. Vousden, K. H., and G. F. Vande Woude. 2000. The ins and outs of p53. *Nat. Cell Biol.* 2:E178–E180.
26. Alexandrova, N., J. Niklinski, V. Bliskovsky, G. A. Otterson, M. Blake, F. J. Kaye, and M. Zajac-Kaye. 1995. The N-terminal domain of c-Myc associates with alpha-tubulin and microtubules *in vivo* and *in vitro*. *Mol. Cell. Biol.* 15:5188–5195.
27. Dong, C., Z. Li, R. Jr. Alvarez, X. H. Feng, and P. J. Goldschmidt-Clermont. 2000. Microtubule binding to Smads may regulate TGF beta activity. *Mol. Cell.* 5:27–34.
28. Ziegelbauer, J., B. Shan, D. Yager, C. Larabell, B. Hoffmann, and R. Tjian. 2001. Transcription factor MIZ-1 is regulated via microtubule association. *Mol. Cell. Biol.* 8:339–349.
29. Kalab, P., R. T. Pu, and M. Dasso. 1999. The Ran GTPase regulates mitotic spindle assembly. *Curr. Biol.* 9:481–484.
30. Ohba, T., M. Nakamura, H. Nishitani, and T. Nishimoto. 1999. Self-organization of microtubule asters induced in *Xenopus* egg extracts by GTP-bound Ran. *Science*. 284:1356–1358.
31. Carazo-Salas, R. E., O. J. Gruss, I. W. Mattaj, and E. Karsenti. 2001. Ran-GTP coordinates regulation of microtubule nucleation and dynamics during mitotic-spindle assembly. *Nat. Cell Biol.* 3:228–234.
32. Nachury, M. V., T. J. Maresca, W. C. Salmon, C. M. Waterman-Storer, R. Heald, and K. Weis. 2001. Importin beta is a mitotic target of the small GTPase ran in spindle assembly. *Cell.* 104:95–106.
33. Wiese, C., A. Wilde, M. S. Moore, S. A. Adam, A. Merdes, and Y. Zheng. 2001. Role of importin-beta in coupling ran to downstream targets in microtubule assembly. *Science.* 291:653–656.
34. Ciciarello, M., R. Mangiacasale, C. Thibier, G. Guarguaglini, E. Marchetti, B. Di Fiore, and P. Lavia. 2004. Importin beta is transported to spindle poles during mitosis and regulates Ran-dependent spindle assembly factors in mammalian cells. *J. Cell Sci.* 117:6511–6522.
35. Parsons, S. F., and E. D. Salmon. 1997. Microtubule assembly in clarified *Xenopus* egg extracts. *Cell Motil. Cytoskeleton*. 36:1–11.
36. Allan, V. J. 1998. Organelle motility and membrane network formation in metaphase and interphase cell-free extracts. *Methods Enzymol*. 298: 339–353.
37. Allan, V. J., and R. D. Vale. 1991. Cell cycle control of microtubule-based membrane transport and tubule formation *in vitro*. *J. Cell Biol.* 113:347–359.
38. Lane, J., and V. Allan. 1998. Microtubule-based membrane motility. *Biochim. Biophys. Acta*. 1376:27–55.
39. Salman, H., Y. Gil, R. Granek, and M. Elbaum. 2002. Microtubules, motor proteins, and anomalous mean squared displacements. *Chem. Phys*. 284:389–397.
40. Reinsch, S., and E. Karsenti. 1997. Movement of nuclei along microtubules in *Xenopus* egg extracts. *Curr. Biol.* 7:211–214.
41. Theriot, J. A., J. Rosenblatt, D. A. Portnoy, P. J. Goldschmidt-Clermont, and T. J. Mitchison. 1994. Involvement of profilin in the actin-based motility of L. monocytogenes in cells and in cell-free extracts. *Cell*. 76:505–517.
42. Christie, P. J., J. E. Ward, S. C. Winans, and E. W. Nester. 1988. The *Agrobacterium tumefaciens* virE2 gene product is a single-stranded-DNA-binding protein that associates with T-DNA. *J. Bacteriol*. 170: 2659–2667.
43. Citovsky, V., M. L. Wong, and P. Zambryski. 1989. Cooperative interaction of *Agrobacterium* VirE2 protein with single-stranded DNA: implications for the T-DNA transfer process. *Proc. Natl. Acad. Sci. USA*. 86:1193–1197.
44. Citovsky, V., B. Guralnick, M. N. Simon, and J. S. Wall. 1997. The molecular structure of *Agrobacterium* VirE2-single stranded DNA complexes involved in nuclear import. *J. Mol. Biol.* 271:718–727.
45. Abu-Arish, A., D. Frenkiel-Krispin, T. Fricke, T. Tzfira, V. Citovsky, S. G. Wolf, and M. Elbaum. 2004. Three-dimensional reconstruction of *Agrobacterium* VirE2 protein with single-stranded DNA. *J. Biol. Chem.* 279:25,359–363.
46. Zupan, J. R., V. Citovsky, and P. Zambryski. 1996. *Agrobacterium* VirE2 protein mediates nuclear uptake of single-stranded DNA in plant cells. *Proc. Natl. Acad. Sci. USA*. 93:2392–2397.
47. Tzfira T., J. Li, B. Lacroix, and V. Citovsky. 2004. *Agrobacterium* T-DNA integration: molecules and models. *Trends Genet*. 20:375–83.
48. Guralnick, B., G. Thomsen, and V. Citovsky. 1996. Transport of DNA into the nuclei of *Xenopus* oocytes by a modified VirE2 protein of *Agrobacterium*. *Plant Cell*. 8:363–373.
49. Tzfira, T., M. Vaidya, and V. Citovsky. 2001. VIP1, an *Arabidopsis* protein that interacts with *Agrobacterium* VirE2, is involved in VirE2 nuclear import and *Agrobacterium* infectivity. *EMBO J*. 20:3596–3607.
50. Newmeyer, D. D., and K. L. Wilson. 1991. Egg extracts for nuclear import and nuclear assembly reactions. *Methods Cell Biol*. 36:607–634.
51. Newmeyer, D. D., and D. J. Forbes. 1988. Nuclear import can be separated into distinct steps in vitro: nuclear pore binding and translocation. *Cell*. 52:641–653.
52. Newmeyer, D. D., D. R. Finlay, and D. J. Forbes. 1986. *In vitro* transport of a fluorescent nuclear protein and exclusion of nonnuclear proteins. *J. Cell Biol.* 103:2091–2102.
53. Finlay, D. R., and D. J. Forbes. 1990. Reconstitution of biochemically altered nuclear pores: transport can be eliminated and restored. *Cell.* 60:17–29.
54. Ullman, K. S., and D. J. Forbes. 1995. RNA polymerase III transcription in synthetic nuclei assembled *in vitro* from defined DNA templates. *Mol. Cell. Biol.* 15:4873–4883.
55. Pu, R. T., and M. Dasso. 1997. The balance of RanBP1 and RCC1 is critical for nuclear assembly and nuclear transport. *Mol. Biol. Cell.* 8:1955–1970.
56. Hughes, M., C. Zhang, J. M. Avis, C. J. Hutchison, and P. R. Clarke. 1998. The role of the ran GTPase in nuclear assembly and DNA replication: characterisation of the effects of Ran mutants. *J. Cell Sci.* 111: 3017–3026.
57. Wang, Z., S. Khan, and M. P. Sheetz. 1995. Single cytoplasmic dynein molecule movements: characterization and comparison with kinesin. *Biophys. J.* 69:2011–2023.
58. King, S. J., and T. A. Schroer. 2000. Dynactin increases the processivity of the cytoplasmic dynein motor. *Nat. Cell Biol.* 2:20–24.
59. Paschal, B. M., H. S. Shpetner, and R. B. Vallee. 1987. MAP 1C is a microtubule-activated ATPase which translocates microtubules in vitro and has dynein-like properties. *J. Cell Biol.* 105:1273–1282.
60. Lasek, R. J., and S. T. Brady. 1985. Attachment of transported vesicles to microtubules in axoplasm is facilitated by AMP-PNP. *Nature*. 316:645–647.
61. Vale, R. D., T. S. Reese, and M. P. Sheetz. 1985. Identification of a novel force-generating protein, kinesin, involved in microtubule-based motility. *Cell*. 42:39–50.
62. Shimizu, T. 1995. Inhibitors of the dynein ATPase and ciliary or flagellar motility. *Methods Cell Biol*. 47:497–501.
63. Heald, R., R. Tournebize, T. Blank, R. Sandaltzopoulos, P. Becker, A. Hyman, and E. Karsenti. 1996. Self-organization of microtubules into bipolar spindles around artificial chromosomes in *Xenopus* egg extracts. *Nature*. 382:420–425.

64. Waterman-Storer, C., D. Y. Duey, K. L. Weber, J. Keech, R. E. Cheney, E. D. Salmon, and W. M. Bement. 2000. Microtubules remodel actomyosin networks in *Xenopus* egg extract via two mechanisms of f-actin transport. *J. Cell Biol.* 150:361–376.

65. Mason, T. G., and D. A. Weitz. 1995. Optical measurements of frequency-dependent linear viscoelastic moduli of complex fluids. *Phys. Rev. Lett.* 74:1250–1253.

66. Amblard, F., A. C. Maggs, B. Yurke, A. N. Pargellis, and S. Leibler. 1996. Subdiffusion and anomalous local viscoelasticity in actin networks. *Phys. Rev. Lett.* 77:4470–4473.

67. Mason, T. G., K. Ganesan, J. H. van Zanten, D. Wirtz, and S. C. Kuo. 1997. Particle tracking microrheology of complex fluids. *Phys. Rev. Lett.* 79:3282–3285.

68. Palmer, A., T. G. Mason, J. Xu, S. C. Kuo, and D. Wirtz. 1999. Diffusing wave spectroscopy microrheology of actin filament networks. *Biophys. J.* 76:1063–1071.

69. Blocker, A., F. F. Severin, J. K. Burkhardt, J. B. Bingham, H. R. Yu, J. C. Olivo, T. A. Schroer, A. A. Hyman, and G. Griffiths. 1997. Molecular requirements for bi-directional movement of phagosomes along microtubules. *J. Cell Biol.* 137:113–129.

70. Lin, S. X. H., K. L. Ferro, and C. A. Collins. 1994. Cytoplasmic dynein undergoes redistribution concomitant with phosphorylation of the heavy chain in response to serum starvation and okadaic acid. *J. Cell Biol.* 127:1009–1019.

71. Sheetz, M. P. 1999. Motor and cargo interactions. *Eur. J. Biochem.* 262:19–25.

72. Valentine, M. T., Z. E. Perlman, T. J. Mitchison, and D. A. Weitz. 2005. Mechanical properties of *Xenopus* egg cytoplasmic extracts. *Biophys. J.* 88:680–689.

73. Caspi, A., R. Granek, and M. Elbaum. 2002. Diffusion and directed motion in cellular transport. *Phys. Rev. E.* 66:011916.

74. Luby-Phelps, K. 2000. Cytoarchitecture and physical properties of cytoplasm: volume, viscosity, diffusion, intracellular surface area. *Int. Rev. Cytol.* 192:189–221.

75. Nieuwenhuizen, T. M., S. Klumpp, and R. Lipowsky. 2004. Random walks of molecular motors arising from diffusional encounters with immobilized filaments. *Phys. Rev. E.* 69:061911.

76. Zumofen, G., J. Klafter, and A. Blumen. 1990. Enhanced diffusion in random velocity-fields. *Phys. Rev. A.* 42:4601–4608.